Electrochemical impedance spectroscopy study on polysulfone/g-C$_3$N$_4$ composite membrane during the separation process

Jieyu Liu[a], Qing Huang[a], Zhe Chen[a],*, Lei Yao[b], Long Huang[c], Changji Dong[c], Lihui Niu[c], Yong Zhang[a],*

[a]*Hubei Key Laboratory of Plasma Chemical and Advanced Materials & School of Materials Science and Engineering, Wuhan Institute of Technology, Wuhan 430205, China, Tel. +86 87195661; emails: zrickchen@163.com (Z. Chen), zhangyong_20191@163.com (Y. Zhang), 1256545530@qq.com (J. Liu), 635442574@qq.com (Q. Huang)*
[b]*School of Electrical and Information Engineering, Wuhan Institute of Technology, Wuhan 430205, China, email: LYAO1@e.ntu.edu.sg (L. Yao)*
[c]*Key Laboratory of Qinghai Salt Lake Resources Comprehensive Utilization, Qinghai Salt Lake Industry Co. Ltd., Golmud 816000, China, emails: huanglong_20191@163.com (L. Huang), dongchangji_20191@163.com (C. Dong), niulihui_20191@163.com (L. Niu)*

ABSTRACT

In this paper, electrochemical impedance spectroscopy (EIS) was applied to monitor the polysulfone (PSF)/g-C$_3$N$_4$ composite membrane in pressurized process and irradiation process, respectively. During the pressurized process, the impedance of the composite membrane decreased in the first 4 h and then maintained a constant value, which confirmed that the hole structure exhibited a compaction effect at the first 4 h and then became stable. The impedance of PSF/g-C$_3$N$_4$ composite membrane decreased when the membrane was irradiated in Xe lamp, which suggested the charges were generated due to the light irradiation. These photo-generated charges are responsible for the photocatalytic property of the composite membrane. All the EIS results are in agreement with the results from SEM and photocatalytic phenomena. EIS is a potential technique for monitoring the membrane state during the separation process.

Keywords: Polysulfone; g-C$_3$N$_4$; Hole structure; Electrochemical impedance spectroscopy

1. Introduction

Membrane separation technology has been widely applied in water treatment due to its excellent separation efficiency, easy maintenance, low chemical sludge effluent and compact modular construction [1,2]. Polysulfone (PSF) is one of the widely used materials for separation membrane [3]. Due to the hydrophobicity of PSF, fouling is one of the key problems for PSF membrane. The previous literatures have proved that many nanoparticles such as TiO$_2$, C$_3$N$_4$, Ag, have great potential for the degradation of organic contaminants in water [4,5]. Introducing the photocatalyst into the membrane can endow the antifouling effect to the membrane [6,7]. As a typical photocatalyst, g-C$_3$N$_4$ has a band gap width of 2.7 eV, which is much narrower than TiO$_2$. In this case, g-C$_3$N$_4$ can exhibit photocatalytic property under visible light irradiation [8,9].

* Corresponding authors.

During the practical separation process, it is important to monitor the membrane state to decide when to interrupt the separation process for the membrane cleaning process. Therefore, a method which can in situ monitor the membrane state is demanded for membrane technology.

Electrochemical impedance spectroscopy (EIS) is a powerful technique to evaluate the microstructure of polymer materials [10,11]. This method can distinguish different membrane states, such as fouling extent on membrane surface [12,13], varying holes in the membrane matrix [14,15], and so on. During the measurement, EIS can probe the sample with an alternating current (AC) signal, which is a non-destructive method. Besides, during the EIS measurement, the sample should be immersed in electrolyte, which can be completely satisfied by the membrane separation apparatus. Moreover, the charge transfer due to the photocatalytic property of nanoparticles can be evaluated by electrochemical techniques [16,17]. So EIS can be potentially used as an in-situ method to evaluate the membrane state during the separation process. In fact, EIS has been successfully utilized to probe the hole structure in membrane [18,19]. However, for an in situ method, it is necessary to analyze any other factors that would influence the result during the measurement.

In this study, the PSF/g-C$_3$N$_4$ composite membranes were prepared and pressurized and then irradiated in Xe lamp. The effects of pressurized process and irradiation on the EIS results have been carefully studied.

2. Experimental

2.1. Preparation of g-C$_3$N$_4$

Urea around 10 g was placed in a crucible of alumina with a cover. It was heated from room temperature to 550°C at the speed of 10°C/min, and then maintained at 550°C for 2 h. The resultant product was cooled in air and ground before use.

2.2. Preparation of PSF/g-C$_3$N$_4$ composite membrane

g-C$_3$N$_4$ power was prepared by pyrolysis of urea. The obtained powder was put in N-methyl pyrrolidone (NMP) and sonicated for 10 min to disperse evenly. After that, PSF power was added into the mixture, and it was stirred in a water bath for 6 h at 60°C. Finally, the solution was casted on a glass plate with a 400-μm casting knife.

2.3. Compaction of PSF/g-C$_3$N$_4$ composite membrane

PSF/g-C$_3$N$_4$ composite membrane was placed in a filtration process with the operation pressure of 0.5 MPa. The feeding side is pure water. The sample was probed by EIS once an hour.

2.4. Photocatalytic property of PSF/g-C$_3$N$_4$ composite membrane

The PSF/g-C$_3$N$_4$ composite membrane was immersed in RhB solution for 6 h in dark, and then irradiated in Xe light. The absorbance of the RhB solution was measured by UV-visible spectrophotometer (RDL8025, Shanghai Youke

Instrument Co. Ltd., China)) once an hour to evaluate the photocatalytic property.

2.5. Characterization

The EIS data were collected on an electrochemical work station (CS310H, Corrtest, China). The electrolyte solution was 0.1 mol L^{-1} KCl aqueous solution. The electrodes are glassy carbon electrode and ITO glass. PSF/g-C$_3$N$_4$ composite membrane was measured by EIS in a membrane cell as our previous literature [20,21].

To probe the membrane state in irradiation, EIS measurement was designed as the following. The membrane cell was placed under the Xe lamp. First, the Xe lamp was turned on for 30 min and then turned off. The membrane/electrolyte system was probed by EIS continuously from the beginning.

The morphology of the membrane was characterized using a field emission scanning electron microscope (SU8020 Hitachi, Japan). The X-ray diffraction pattern was measured by XRD (D8 advance, Bruker, Germany).

3. Results and discussion

3.1. Microstructure of PSF/g-C$_3$N$_4$ composite membrane

As shown in Fig. 1, there is a strong diffraction peak at 27.5°, which is the characteristic peak of the stacking of g-C$_3$N$_4$ layers, corresponding to the crystal plane of (002). It is proved that the powder has a graphene-like layered structure. Another diffraction peak at 13.1° is the characteristic peak of the repeated unit C$_6$N$_7$ ring in the structure of 3, s-triazine, and the crystal plane is (100) [22–24]. The structure of 3, s-triazine belongs to g-C$_3$N$_4$.

It can be seen from Fig. 2 that PSF/g-C$_3$N$_4$ composite membrane exhibited general microstructure of pure polysulfone membrane [25]. Figs. 2a and b illustrate that a large number of rectangular and triangular g-C$_3$N$_4$ particles are on the surface of the membrane, with an average size of 0.2 μm. Figs. 2c and d show that there are many small pores in the surface thin layer and finger-like holes in the supporting layer. A small number of g-C$_3$N$_4$ particles are attached to the wall of finger-shaped channels, which are labeled in Fig. 2d in red rectangles.
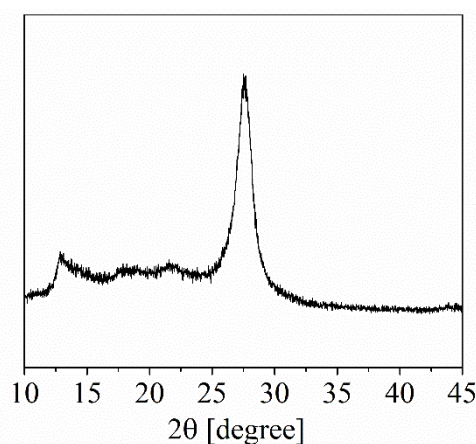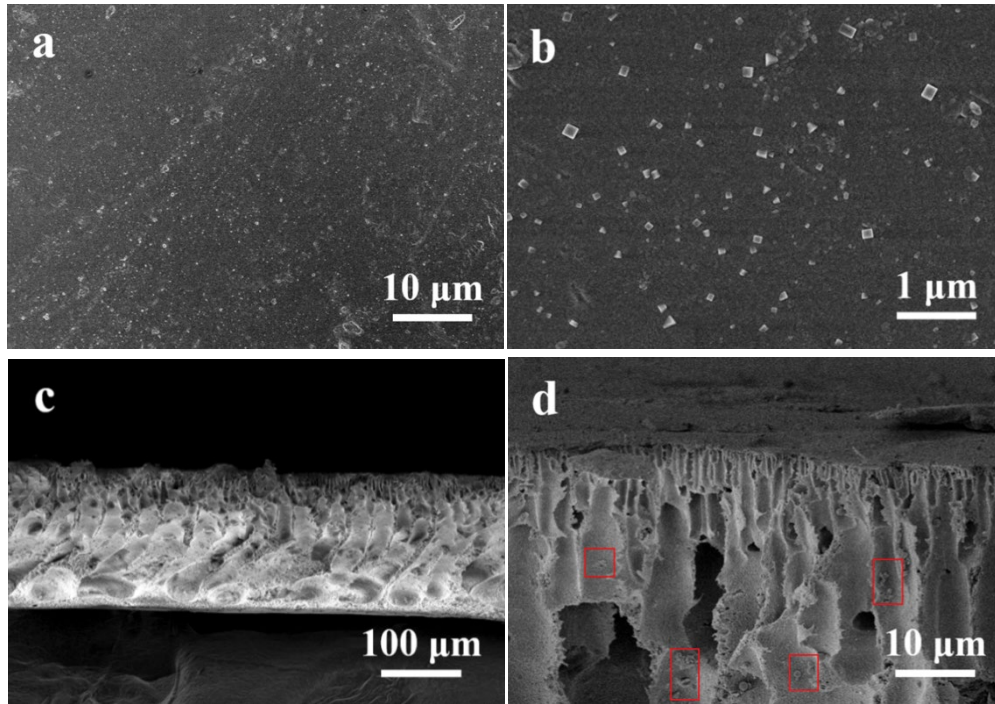

Fig. 1. XRD pattern of prepared g-C$_3$N$_4$.

Fig. 2. SEM images of PSF/g-C$_3$N$_4$ composite membrane. (a,b) Surface of membrane. (c,d) Cross section of membrane.

3.2. PSF/g-C$_3$N$_4$ composite membrane in pressurized process

It can be clearly found in Fig. 3 that semicircle in the Nyquist plot enlarges sharply with increasing pressurized time from 0 to 4 h, and then becomes unchanged. This means that the impedance increases sharply at the first 4 h.

For a membrane, the electrolyte in the membrane holes is responsible for charge conductance, while the membrane bulk acts as the capacitance. The capacitance of the composite membrane satisfies Eq (1) that is the parallel connection in membrane. And the resistance of PSF/g-C$_3$N$_4$ composite membrane satisfies Eq. (3) that is the parallel connection of each hole channel in membrane.

$$C_m = \sum_1^n \left(C_1 + C_2 + ... + C_n \right) \tag{1}$$

where C_m is the capacitance of membrane and C_n is the capacitance of membrane bulk part between each hole channel.

$$C_n = \frac{\varepsilon_0 \varepsilon_m A_b}{\delta} \tag{2}$$

where ε_0 is the dielectric constant of vacuum, ε_m is the dielectric constant of membrane, A_b is the effective area of membrane bulk and δ is the thickness of membrane.

$$\frac{1}{R_m} = \sum_1^n \left(\frac{1}{R_1} + \frac{1}{R_2} + ... + \frac{1}{R_n} \right) \tag{3}$$

where R_m is the resistance of membrane and R_n is the resistance of each hole channel in membrane, A_h is the effective area of the holes and δ is the thickness of membrane.
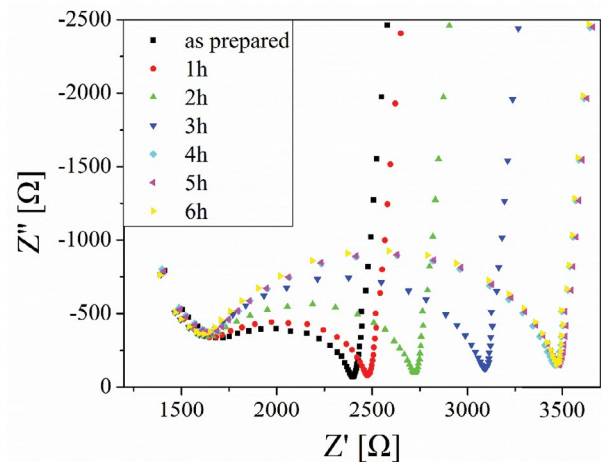

Fig. 3. Nyquist plots of PSF/g-C$_3$N$_4$ composite membrane pressurized for 1 h, 2 h, 3 h, 4 h, 5 h, 6 h and as prepared.

$$R_n = \frac{\rho \delta}{A_h} \tag{4}$$

where ρ is the resistivity of electrolyte.

In this case, the equivalent circuit adapted for present membrane/electrolyte system can be expressed as $(R_m{-}C_m)R_e$ (Fig. 4a), where R_e is associated to the electrolyte resistance, while R_m and C_m refer to the resistance and capacitance of the membrane. The fitted values of R_m and C_m for the impedance plots according to the equivalent circuit are shown in Table 1.

Generally, polymer materials would be compact during the pressurized process, resulting in the shrinkage of hole
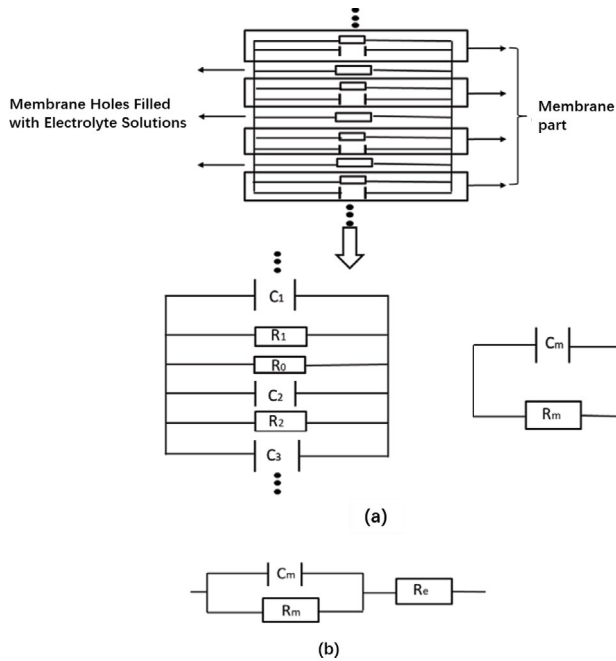
Fig. 4. Equivalent circuit of membrane.

Table 1
Capacitance and resistance of PSF/g-C$_3$N$_4$ composite membrane for different pressurized time fitted according to the equivalent circuit in Fig. 4b
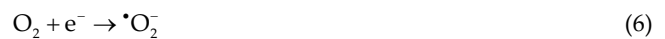
Pressurized time (h)	C_m (F)	R_m (Ω)
0	4.63×10^{-9}	817
1	4.82×10^{-9}	911
2	5.19×10^{-9}	1,143
3	5.22×10^{-9}	1,497
4	5.35×10^{-9}	1,814
5	5.36×10^{-9}	1,831
6	5.41×10^{-9}	1,868

structure. The effective area of the membrane bulk becomes larger as the holes shrink when the membrane is in the pressurized process. This would lead to the increase of the membrane capacitance and hole resistance, according to Eqs. (2) and (4). As shown in Table 1, the capacitance and resistance of PSF/g-C$_3$N$_4$ composite membrane increase sharply at the first 4 h, and then arrive at a saturated value. It could be the holes in the composite membrane shrink in the first 4 h and then become stable.

Bode plots shown in Fig. 5 indicate that the impedance of the system gradually increases with pressurized time in the first 4 h and then stabilizes after 4 h, which is consistent with the fitted value.

3.3. PSF/g-C$_3$N$_4$ composite membrane in Xe irradiation

Under the excitation of photons, electrons in the energy band of g-C$_3$N$_4$ can move from valence band to conduction band and form electron–hole pairs. The specific reaction process is as follows:

$$g - C_3N_4 \xrightarrow{\text{irradiation}} e^- + h^+ \tag{5}$$

$$O_2 + e^- \rightarrow {}^\bullet O_2^- \tag{6}$$

$${}^\bullet O_2^- + e^- + 2H^+ \rightarrow H_2O_2 \tag{7}$$

$$H_2O_2 + e^- \rightarrow {}^\bullet OH + OH^- \tag{8}$$

These reactions produce many active radicals, accompany with photo-generated charges. These radicals can degrade the organics, thus endow the antifouling property to the composite membrane. RhB solution was utilized to evaluate the antifouling effect. The degradation of RhB by composite membrane is shown in Fig. 6. And the slope of the line is the kinetic constant.

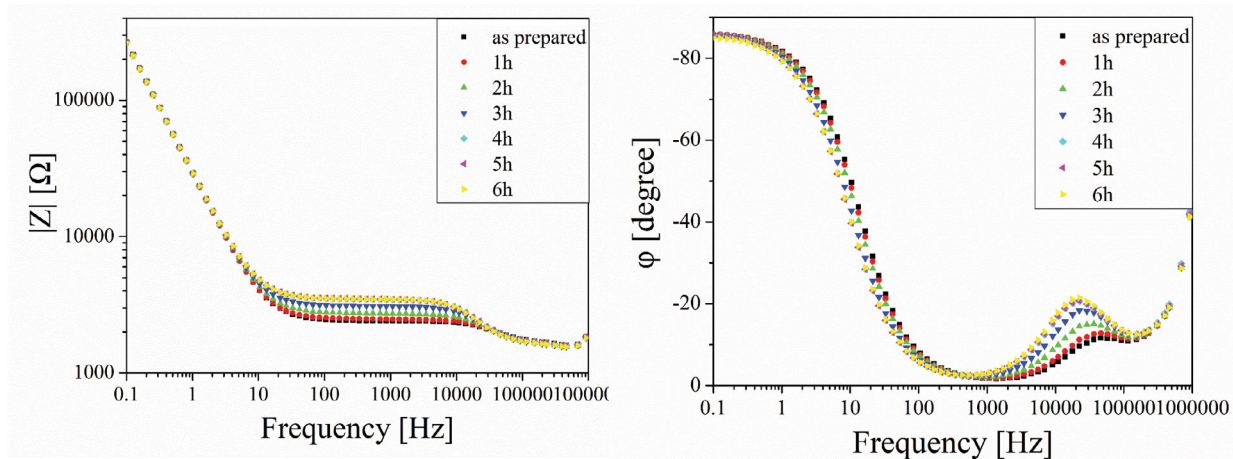According to the theory of Langmuir–Hinshelwood model [26]:

Fig. 5. Bode plots of PSF/g-C$_3$N$_4$ composite membrane pressurized for 1 h, 2 h, 3 h, 4 h, 5 h, 6 h and as prepared.
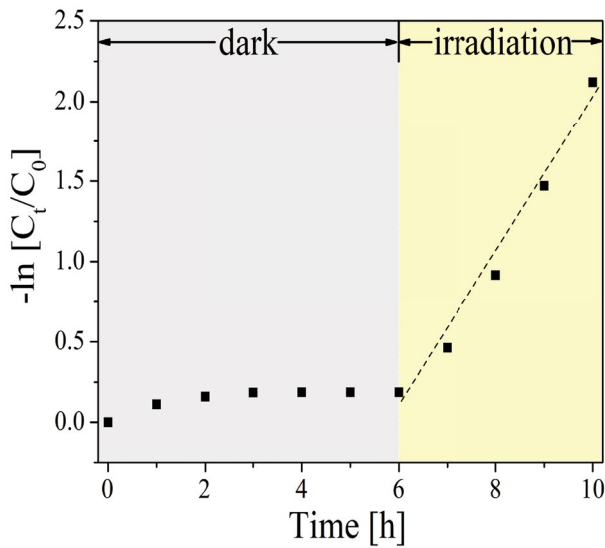
Fig. 6. Kinetic simulation of first-order reaction for light degradation of RhB.

$$r = -\frac{dC_s}{dt} = \frac{k_r K C_s}{\left(1 + K C_s\right)} \tag{9}$$

where C_s is the concentration of reactant, t is the reaction time, k_r is the constant of reaction rate and K is the constant of reactant adsorption.

When the reactant concentration is low, $KC_s \ll 1$ and can be negligible. When $t = 0$ and $C_s = C_0$ were substituted into Eq. (9), the following equation was obtained :

$$-\ln\left(\frac{C_t}{C_0}\right) = kt \tag{10}$$

where C_0 is the initial concentration of reactant, C_t is the concentration of reactant after reaction and K is the kinetic constant.

The results show that the photocatalytic reaction conforms to the law of first-order reaction kinetics. The straight line was fitted according to Eq. (10). The photocatalytic
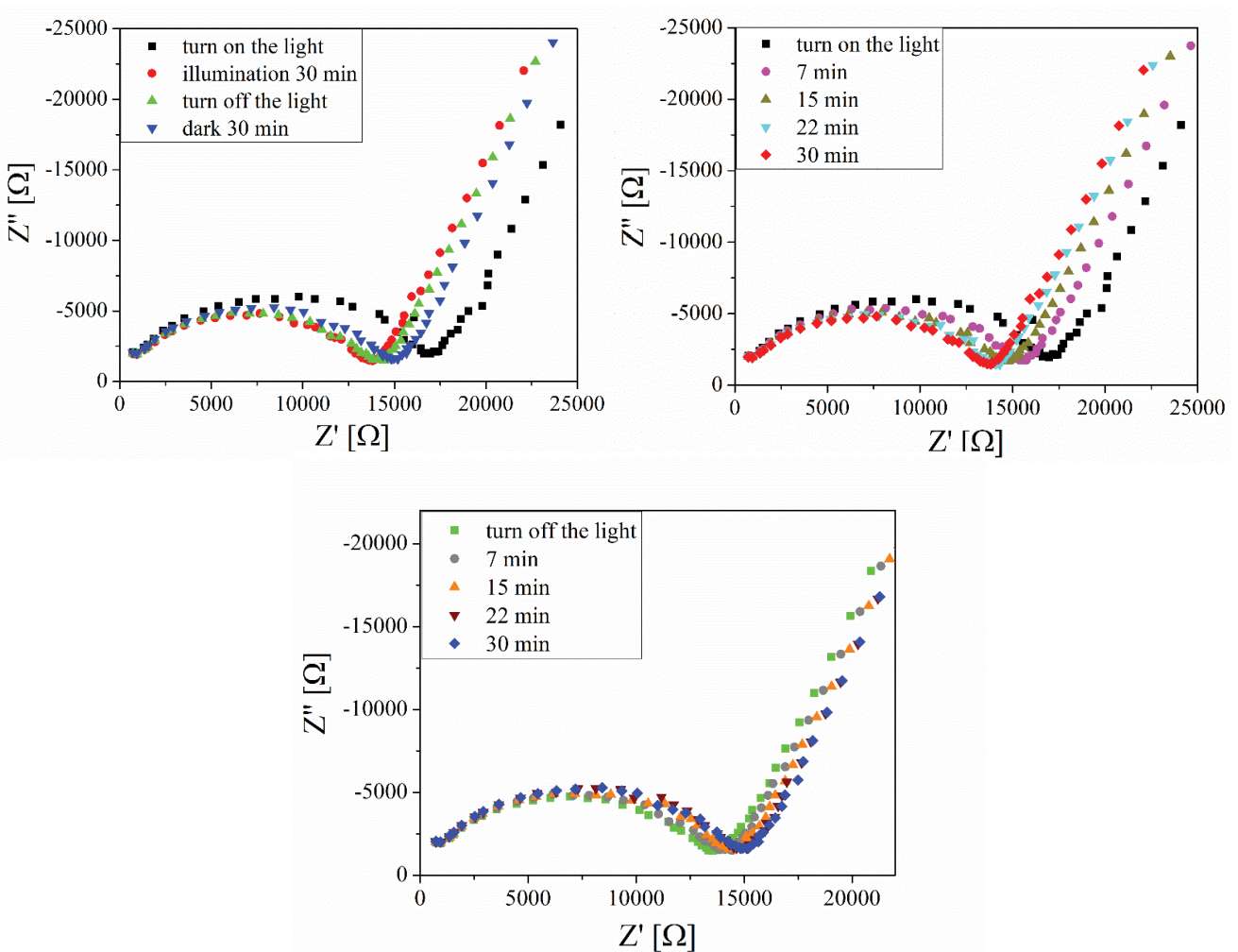

Fig. 7. Nyquist plots of PSF/g-C₃N₄ composite membrane under light condition and dark condition.

rate $k = 9.17 \times 10^{-3}$ min^{-1} can be obtained by calculating the slope of the straight line simulated by the first-order reaction kinetics.

During the photocatalytic process, three common active oxidant species, hydroxyl radicals ($^\bullet$OH), hole (h$^+$) and superoxide radical ($^\bullet$O$_2^-$), would be formed and the electron transferring would occur around the photocatalysts [27–29]. The photo-generated electron–hole pairs are responsible for the photocatalytic reaction [30]. To further investigate the photocatalytic mechanism of the composite membrane, EIS coupled with Xe irradiation was utilized to detect the photo-generated carriers. The Xe lamp was turned on for 30 min and then turned off. The membrane/electrolyte system was continuously probed by EIS, and the results are shown in Fig. 7.

When the light was turned on, the impedance of PSF/g-C$_3$N$_4$ composite membrane clearly decreased and finally reached stability. That should be due to the formation of electron–hole pairs and the reaction between photo-generated electrons with holes in electrolyte solution, resulting in photo-generated charges such as $^\bullet$O$_2^-$, OH$^-$. The results show that the catalytic reaction mainly takes place in the holes of the membrane, which means the photo-generated charge mainly transports in the hole channels. And the generation and recombination of photo-generated charges exist in the holes of the membrane at the same time. When the generation rate is higher than the recombination rate of photo-generated charges, the charge concentration in the hole channels increases, so the impedance decreases. After illuminating 30 min, the generation and recombination of photo-to-generated charges arrived at equilibrium. When the light was turned off, the catalytic reaction ended and the photo-to-generated charges were no longer produced. But there were still a number of photo-generated charges remained in the hole channels. So the impedance of the system is still smaller than the original one. The recombination of charges is predominant in this process, resulting in the slight increase of impedance.

4. Conclusions

PSF/g-C$_3$N$_4$ composite membrane was prepared in this study. EIS method was utilized to evaluate the membrane in the pressurized process and photo catalytic process. It was found that the impedance of the composite membrane increased at the first 4 h and then arrived a saturated value, which meant a compact effect of the hole structure in the first 4 h. The photo-generated charges were detected by EIS when the composite membrane was irradiated by Xe lamp. The membrane impedance decreased due to the influence of photo-generated charges, which confirmed that the photo-to-generated charges mainly existed in the hole channels of the membrane. The above results suggested that EIS is a potentially powerful technique, which can in situ monitor the membrane state during the separation process.

Acknowledgments

References

[1] A. Lee, J.W. Elam, S.B. Darling, Membrane materials for water purification: design, development, and application, Environ. Sci. Water Res., 2 (2016) 17–42.

[2] Q. Chen, Y.Y. Liu, C. Xue, Y.L. Yang, W.M. Zhang, Energy self-sufficient desalination stack as a potential fresh water supply on small islands, Desalination, 359 (2015) 52–58.

[3] M. Padaki, R.S. Murali, M.S. Abdullah, N. Misdan, A. Mosleh-yani, M.A. Kassim, N. Hilal, A.F. Ismail, Membrane technology enhancement in oil-water separation, a review, Desalination, 357 (2015) 197–207.

[4] W.X. Zeng, Y. Bian, S. Cao, Y.J. Ma, Y. Liu, A.Q. Zhu, P.F. Tan, J. Pan, Phase transformation synthesis of strontium tantalum oxynitride-based heterojunction for improved visible light-driven hydrogen evolution, ACS Appl. Mater. Interfaces, 10 (2018) 21328–21334.

[5] Y.J. Ma, J. Jiang, A.Q. Zhu, P.F. Tan, Y. Bian, W.X. Zeng, H. Cui, J. Pan, Enhanced visible-light photocatalytic degradation by Mn$_3$O$_4$/CeO$_2$ heterojunction: a Z-scheme system photocatalyst, Inorg. Chem. Front., 5 (2018) 2579–2586.

[6] J. Lu, Y. Qin, Q. Zhang, C. Yu, Y. Wu, Y. Yan, H. Fan, M. Meng, C. Li, Antibacterial, high-flux and 3D porous molecularly imprinted nanocomposite sponge membranes for cross-flow filtration of emodin from analogues, Chem. Eng. J., 360 (2019) 483–493.

[7] J. Lu, Y. Wu, X. Lin, J. Gao, H. Dong, L. Chen, Y. Qin, L. Wang, Y. Yan, Anti-fouling and thermosensitive ion-imprinted nanocomposite membranes based on graphene oxide and silicon dioxide for selectively separating europium ions, J. Hazard. Mater., 353 (2018) 244–253.

[8] F. Dong, Z. Wang, Y.J. Sun, W.K. Ho, H.D. Zhang, Engineering the nanoarchitecture and texture of polymeric carbon nitride semiconductor for enhanced visible light photocatalytic activity, J. Colloid Interface Sci., 401 (2013) 70–79.

[9] X. Zhang, X. Xie, H. Wang, J. Zhang, B. Pan, Y. Xie, Enhanced photo responsive ultrathin graphitic-phase C$_3$N$_4$ nanosheets for bioimaging, J. Am. Chem. Soc., 135 (2012) 18–21.

[10] S.M.R. Niya, M. Hoorfar, Study of proton exchange membrane fuel cells using electrochemical impedance spectroscopy technique – a review, J. Power Sources, 240 (2013) 282–293.

[11] C. Yin, S. Wang, Y.J. Zhang, Z. Chen, Z.D. Lin, P. Fu, L. Yao. Correlation between the pore resistance and water flux of the cellulose acetate membrane, Environ. Sci. Water Res., 3 (2017) 1037–1041.

[12] Z.J. Zhao, S.Y. Shi, H.B. Cao, Y.P. Li. Electrochemical impedance spectroscopy and surface properties characterization of anion exchange membrane fouled by sodium dodecyl sulfate, J. Membr. Sci., 530 (2017) 220–231.

[13] T.C. Chilcott, A. Antony, G. Leslie, In situ electrical impedance characterization of fouling by calcium agents in reverse osmosis membrane systems using Maxwell Wagner and hydrodynamic models, Desalination, 403 (2017) 64–79.

[14] J.Y. Liu, Z. Chen, L. Yao, J.J. Li, J.S. Zhang, Q.M. Fu, C.Q. He, P.F. Fang, Correlation between the ion permeation and free volume property in ethyl cellulose film during the acid treatment, Mater. Chem. Front., 3 (2019) 1518–1522.

[15] Q. Huang, Q.Z. Luo, Z. Chen, L. Yao, P. Fu, Z.D. Lin, The effect of electrolyte concentration on electrochemical impedance for evaluating polysulfone membrane, Environ. Sci. Water Res., 4 (2018) 1145–1151.

[16] H.M. Wang, S.B. Naghadeh, C.H. Li, V.L. Cherrette, P.F. Fang, K. Xu, J.Z. Zhang, Enhanced photoelectrochemical and photocatalytic properties of CdS nanowires decorated with Ni$_3$S$_2$ nanoparticles under visible light irradiation, J. Electrochem. Soc., 166 (2019) H3146–H3153.

[17] H.M. Wang, C.H. Li, P.F. Fang, Z.L. Zhang, J.Z. Zhang, Synthesis, properties, and optoelectronic applications of two-dimensional MoS$_2$ and MoS$_2$-based heterostructures, Chem. Soc. Rev., 47 (2018) 6101–6127.

[18] Y. Jing, B.P. Chaplin, Electrochemical impedance spectroscopy study of membrane fouling characterization at a conductive sub stoichiometric TiO$_2$ reactive electrochemical membrane:

transmission line model development, J. Membr. Sci., 511 (2016) 238–249.

[19] F.W. Liu, M.X. Yin, B.Y. Xiong, F. Zheng, W.F. Mao, Z. Chen, C.Q. He, X.P. Zhao, P.F. Fang, Evolution of microstructure of epoxy coating during UV degradation process studied by slow positron annihilation spectroscopy and electrochemical impedance spectroscopy, Electrochim. Acta, 133 (2014) 283–293.

[20] Y.J. Zhang, Z. Chen, L. Yao, X Wang, P. Fu, Z.D. Lin, The graphene oxide membrane immersing in the aqueous solution studied by electrochemical impedance spectroscopy, Mater. Res. Express, 5 (2018) 045606.

[21] J.Y. Liu, Z. Chen, L. Yao, S.G. Wang, L. Huang, C.J. Dong, L.H. Niu, The 2D platelet confinement effect on the membrane hole structure probed by electrochemical impedance spectroscopy, Electrochem. Commun., 106 (2019) 106517.

[22] J. Liu, T. Zhang, Z. Wang, G. Dawson, W. Chen, Simple pyrolysis of urea into graphitic carbon nitride with recyclable adsorption and photocatalytic activity, J. Mater. Chem., 21 (2011) 14398–14401.

[23] B. Li, M. Meng, Y. Cui, Y. Wu, Y. Zhang, H. Dong, Z. Zhu, Y. Feng, C. Wu, Changing conventional blending photocatalytic membranes (BPMs): focus on improving photocatalytic performance of Fe_3O_4/g-C_3N_4/PVDF membranes through magnetically induced freezing casting method, Chem. Eng. J., 365 (2019) 405–414.

[24] H. Che, L. Liu, G. Che, H. Dong, C. Liu, C. Li, Control of energy band, layer structure and vacancy defect of graphitic carbon nitride by intercalated hydrogen bond effect of NO_3^- toward improving photo catalytic performance, Chem. Eng. J., 357 (2019) 209–219.

[25] W.Q. Zhou, Z. Chen, Q.M. Fu, Y. Zhang, L. Yao, H.J. Zhang, Evaluating the pore structures of polysulfone membranes by positron 3γ-annihilation probability and electrochemical impedance spectroscopy, JOM, 70 (2018) 1920–1923.

[26] K.V. Kumar, K. Porkodi, F. Rocha, Langmuir–Hinshelwood kinetics–a theoretical study, Catal. Commun., 9 (2008) 82–84.

[27] J. Wang, L. Tang, G.M. Zeng, Y.C. Deng, Y. Liu, L. Wang, Y. Zhou, Z. Guo, J.J. Wang, C. Zhang, Atomic scale g-C_3N_4/Bi_2WO_6 2D/2D heterojunction with enhanced photocatalytic degradation of ibuprofen under visible light irradiation, Appl. Catal., B, 209 (2017) 285–294.

[28] L. Tang, C.Y. Feng, Y.C. Deng, G.M. Zeng, J.J. Wang, Y. Liu, H.P. Feng, J.J. Wang, Enhanced photocatalytic activity of ternary Ag/g-C_3N_4/NaTaO$_3$ photocatalysts under wide spectrum light radiation: the high potential band protection mechanism, Appl. Catal., B., 230 (2018) 102–114.

[29] Z.T. Liu, Y. Gao, J. Dong, M.L. Yang, J. Wen, M. Liu, B. Zhang, C. Fang, Y. Zhang, H. Ma, X. Gao, W. Chen, M. Shao, Chlorinated wide bandgap donor polymer enabling annealing free non-fullerene solar cells with the efficiency of 11.5%, J. Phys. Chem. Lett., 9 (2018) 6955–6962.

[30] Y.C. Deng, L. Tang, C. Feng, G.M. Zeng, J. Wang, Y. Zhou, Y. Liu, B. Peng, H.P. Feng, Construction of plasmonic Ag modified phosphorous-doped ultrathin g-C_3N_4 nanosheets/BiVO$_4$ photocatalyst with enhanced visible-near-infrared response ability for ciprofloxacin degradation, J. Hazard. Mater., 344 (2018) 758–769.